ENGINEERING RESEARCH JOURNAL (ERJ)
Vol. 51, No. 4 October. 2022, pp.132-140
Journal Homepage: http://erj.bu.edu.eg

Kinematic Modeling of 4 Mecanum Wheeled Manipulator with 6 DOF

Baher Samy [a *], Saber Abd Raboo [a], Mahmoud Elsamanty [a, b]

[a] Department of Mechanical Engineering, Benha University, Egypt

[b] Mechatronics and Robotics Department, School of Innovative Design, Egypt-Japan University for Science and Technology

* Corresponding author

Abstract

This paper looks at how a mobile manipulator with six degrees of freedom (DOFs) can track the desired trajectory. A motion planning approach is proposed based on examining its kinematics models. The forward and inverse kinematics are analyzed using the Denavit-Hartenberg technique. The end-location effector and orientation are divided into two sections. In the first half, the manipulator provides sub-vectors projected on the Z-axis in the world frame, such as location and orientation. In the second half, the mobile base and manipulator follow the required path and reach the sub-vectors on the world frame's axes X and Y, respectively. The effectiveness of the suggested technique is demonstrated using simulated outcomes.

Keywords : Wheeled mobile robots, Mecanum wheel, Inverse Kinematics.

1. Introduction

A new wave of technology powered by mobile manipulators enables us to be versatile in many filed such as construction, space, production lines, and warehouses. It consists of a robot frame, an arm manipulator, tooling, and vision; it will possess a broad property when omnidirectional or mecanum wheels drive the plate shape. Industrial robots have gradually replaced human power to meet rising demands regarding cost savings, throughput improvement, and personal protection. As a primary research subject in robotics, trajectory planning has gained a great deal of attention over the past several decades since it is crucial to guide a robot toward the intended outcome.[1]

Furthermore, the fundamental problem is dealing with the limitless number of inverse kinematic (IK) solutions that kinematically redundant manipulators may detect. IK is more difficult to analyze due to the nonlinear forward kinematics, which maps all joint angles to the end effector position. It is challenging and difficult to solve the inverse kinematics problem for robotic manipulators. Due to the geometry of the robot and the nonlinear trigonometric equations defining the mapping between Cartesian space and joint space, this task is tough. So, IK is the method of

deciding the individual joint angles for the position and orientation of the end effector. Three alternative approaches may be used to efficiently solve the complicated kinematic structures of redundant real-time manipulators: analytical or closed approaches which is mainly used to solve the robotic arm with a definite configuration, numerical approaches which based on the Jacobi matrix and approximates the optimal solution by numerical iteration, and geometric approaches which has a narrower application than the analytical method. This method solves the inverse kinematic solution of the robotic arm mainly by the geometric configuration of the robotic arm [2]. Manipulators are run in most implementations using a primary method called "Teaching and Play," which requires pre-defining joint angles for various activities. However, the increased sophistication in tasks and manipulator structures increases the manipulators' adaptability and versatility to execute the various tasks. So, calculating mutual positions for the different configurations of the manipulator using Inverse Kinematics (IK) is vital.

Although a closed-form solution to this problem is preferred in many situations, it is difficult to locate one often. For this reason, several other ways of finding a solution to the inverse kinematics problem have been suggested. Moreover, IK can be implemented based on computational solutions, computational algorithms based on optimization techniques, evolutionary computation, or neural networks. The ability of neural networks (NN) to describe nonlinear relationships between input and output data for the manipulator has also long been acknowledged. They are a great choice to map the region between the Cartesian space and the Joint space required by the inverse kinematics issue due to their capacity to learn by doing. The 6-DOF manipulators' inverse kinematics challenge has been approached from several angles. The most popular method is a speed solution based on a closed or iterative Jacobian matrix. These alternatives, however, are scalable and offer a variety of implementations. However, it needs detailed measurements and expansive time costs. In addition, it can contain an accumulation of errors and Jacobian Singularities [3].

Due to their intricate computations, inverse kinematics solutions based on optimization techniques are frequently not suitable for real-time control. Position-based analytical solutions, also known as closed-form solutions, provide superior dependability, higher solution speed, and less computation than speed-based solutions. The positions and DH models of all current 6-DOF manipulators are identical; therefore this methodology is still universal even if the position-based analytical solution method depends on the geometric configuration of the described manipulator. To execute position-based kinematic control, Lee and Bejczy were the first to design a closed-form inverse kinematics solution in 1991. Additionally, they used a parametric method to reduce the size of redundant manipulators, and they verified that the position-based solution outperformed the Jacobian 8-DOF solution based on speed. However, the selection of redundant joints has a significant impact on how effective the approach is [4]. By parameterizing or fixing joint variables at an arbitrary value to convert redundant manipulators to non-redundant ones, Zaplana and Basanez discovered superfluous joints through workspace research [5].

The method can offer analytical answers for duplicate manipulators with several degrees of freedom, but it cannot express the intuitive qualities of redundant motion. For 7-DOF manipulators, Dahm and Joublin proposed a closed-form inverse kinematics method. To describe the elbows self-motion, they included an auxiliary parameter termed "arm angle," from which they deduced the expression of all joints for any desired elbow position. Additionally, they proposed an early technique of joint mapping limitations to the arm's angle. The algorithm, however, does not take the arrangement of the arm multiples into account [6]. Shimizu et al. developed their approach to avoid the kinematic singularity. set the third joint's angle to zero, redefining the reference plane for the angle of the arm. Unfortunately, the approach is unable to actively control gun design [7]. Additionally, Yan et al. suggested a revised definition of the double arm angle and employed two fixed vectors to determine the reference plane's orientation [8]. Although the link between the arm angle and the joint variables has not been seen, the plane created by the two vectors is employed as the reference plane since one of the fixed vectors is aligned with the shoulder wrist vector [9].

This paper presents an exact velocity equation for a kinematic system with Mecanum wheels. A robotic manipulator with six joints is designed for this study. This robot has six degrees of freedom due to the presence of six joints. The assignment of frames to each robot joint is done in accordance with the DH protocol. The DH parameters for the robot built for this analysis. The robot model was created using CAD model definition, which describes the

configuration of the robot body, showing the wheels and frames. The hardware model description shows the motors, controllers, and encoders. Section 2, of this article will describe the kinematic model that composed of four parts, the description of the model arm, the mobile robot model, the integrated model, and the fourth section will be the mathematical model. In section 3, The results obtained from the research are displayed.

2. CAD MODEL

The Mobile manipulator demonstrated in this paper consists of a mobile platform with four mecanum wheels driven by four DC Maxon motors, carrying a 6 DOF arm manipulator driven by stepper motors. The mobile manipulator is shown in Fig.1. The Arm Manipulator was designed in Solid Works, and the assembly was composed of two main parts (mobile robot and arm manipulator). The model design is developed using Solid Works to compute all the needed parameters (mass, center of inertia, dimension). The model is simulated realistically, and all the used parameters are considered based on the physical specifications and following the 3D Solid Works design of the mobile robot.

2.1 Mobile robot

Flexibility to change the geometrical arrangement of the robot fast while using the same parts. The primary design decisions made in relation to the creation of the chassis, engine, and power systems are discussed in this section. The chassis was primarily developed with lightness in mind to lower the amount of energy required to operate the robot. The chassis is composed of aluminium bars and includes a portion that is both light and sturdy. It is designed so that the side rails represent a fixed rail where the wheels are attached so that the wheelbase cannot be changed easily.

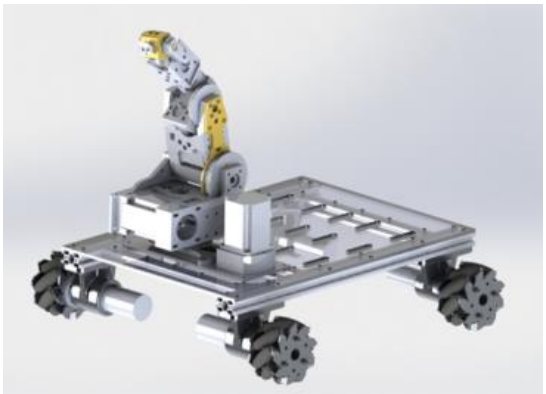

Fig. 1. CAD model of the mobile manipulator

Fig. 2. Fully assembled mecanum wheeled robot.

Additionally, these four bars come together to form a rectangular stiff linkage at which four fixed joints created using a 3D printer may connect four short bars supporting the wheels, allowing for the stability of the robot's course and ground clearance., as shown in Fig. 2.

The maximum permitted longitudinal/lateral terrain slopes are simply deduced given that the robot is equipped with one arm in the front part and that the power system is made up of a Power source positioned in the rear half. In the most crucial configuration, i.e., minimal track and wheelbase and maximum ground clearance, rollover is avoided up to the scenario of a longitudinal or lateral slope of 45 when the maximum front payload, including arm weight, is 15 kg. Four in-wheel electric DC brushless Maxon motors power the mobile robot. To offer more propulsion, the robot was built with rear motors that are more powerful than the front motors. The characteristics of the motor are shown in Table 1 according to the manufacturer.

Table 1. Wheels motor's characteristics.

	Rear Motors	Front Motors
Motor mass	650g	454g
Voltage	48 V	48 V
Power	90 W	60 W
Maximum speed	57 rpm	90 rpm
Tire diameter	6 in	6 in

The wheel motors have several advantages regarding an encoder that allows us to get the best situation in controlling the robot by a feedback loop to minimize the error of velocity and gain the best situation for the robot's path and suitable drivetrain. First, the wheel motors have no transmission required to be connected to the robot wheels. It makes the mechanical design of the vehicle more accessible and more reliable. In addition, it lightens

the load, creating more room above the chassis for a cargo and underneath it for better ground clearance. However, it prevents effects from occurring between parts that could be harmed or harm the environment.

The position measurement tool has been determined to be a Maxon prototype encoder. A sensitivity of 0.3 μV and a resolution of 14 bits define this encoder. The fact that this device doesn't have a mechanical connection between the stator and the rotor (motion is transmitted from the encoder axis to the measuring electronics by utilizing the magnetic effect) also makes it particularly suitable for this application. This feature reduces the risk of disc damages from mechanical vibrations and shocks, which frequently occur when standard encoders are used in off-road vehicles.

2.2. Arm Manipulator

The gripper is fastened to the end of the arm, and the manipulator is perched on top of the robot's base. Denavit Hartenberg (DH) characteristics, as indicated in Table 2, dictate the design of the manipulator. All axes of the revolute joints are perpendicular to the neighboring ones. The first wrist centre point (intersection of axes one, two, and three) serves as the origin of the base frame (xb, yb, zb), and the z-axis is parallel to the first axis. In the home position, which is the position when all joint parameters are equal to zero, the x-axis is perpendicular to the plane that is spanned by the first and second axes. All axes are located in the yz plane in this design. he second wrist center is selected as the origin of the end effector (xe, ye, and ze) frame (intersection of axes five, six, and seven). In the home position, the x-axis is perpendicular to the plane that is divided by axes six and seven and the z-axis is congruent with axis seven. The final row of Table 2 is zero due to this unusual end effector frame selection. However, this entry is still included in the Table to allow for the consistent introduction of symbolic expressions. Fig. 3 provides a visual schematic of the manipulator. Note that the axes of joints one and three and five and seven coincide in this home arrangement.

Table 1. DH parameters.

Link	a_i	α_i	d_i	θ_i
1	a_1	-90	d_1	θ_1
2	a_2	0	0	θ_2
3	a_3	90	0	θ_3
4	0	90	d_4	θ_4
5	0	90	0	θ_5
6	0	0	d_6	θ_6

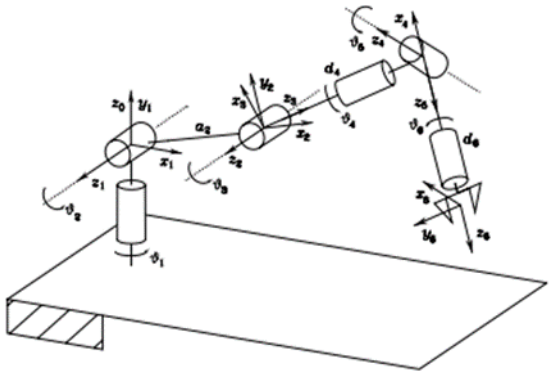

Figure 3 pictorial schematic of the manipulator

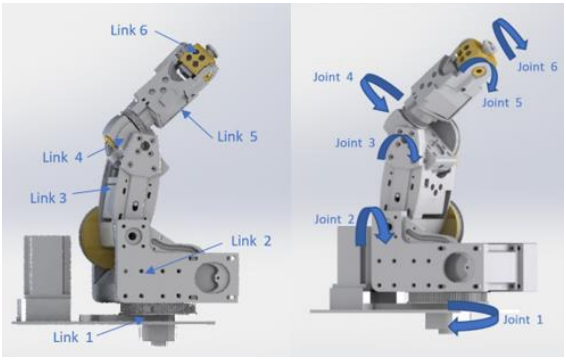

Figure 4. CAD model of the arm manipulator

3. Mathematical Model

The mathematical model is based on the following equations [10]:
The pose of the robot is given by:

$$\xi_1 = \begin{bmatrix} x \\ y \\ \theta \end{bmatrix} \quad (1)$$

$$R(\Theta) = \begin{bmatrix} \cos\theta & \sin\theta & 0 \\ -\sin\theta & \cos\theta & 0 \\ 0 & 0 & 1 \end{bmatrix} \quad (2)$$

The matrix used for mapping global reference -0

$$\dot{\xi} = R(\Theta)\ \dot{\xi}_1 \quad (3)$$

From the equation above, Robots' motion in the inertial frame can be computed easily

$$\dot{\xi}_1 = R(\Theta)^{-1}\ \dot{\xi}_R \quad (4)$$

Forward kinematics model

XR is the positive direction for Robots' forward motion. Let us assume that the velocity of the wheel is

$$\dot{\xi}_1 = \mathrm{R}(\Theta)^{-1} \begin{bmatrix} \frac{r\,\dot{\varphi}_1}{2} + \frac{r\,\dot{\varphi}_2}{2} \\ 0 \\ \frac{r\,\dot{\varphi}_1}{2l} + \frac{-r\,\dot{\varphi}_2}{2l} \end{bmatrix} \quad (5)$$

$$\mathrm{R}(\Theta)^{-1} = \begin{bmatrix} \cos\theta & -\sin\theta & 0 \\ \sin\theta & \cos\theta & 0 \\ 0 & 0 & 1 \end{bmatrix} \quad (6)$$

Wheel Equation and constraint

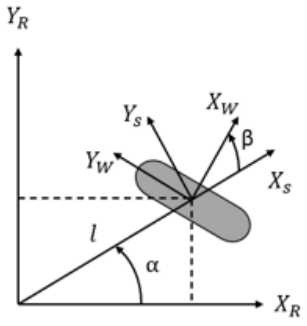

$$v_{IW} = v_{IR} + \omega_{IR} * r_{RS} \quad (7)$$

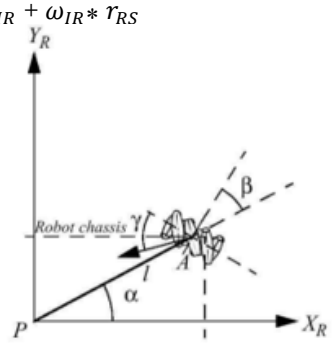

$$\dot{y}_w = r\dot{\varphi}\cos(\gamma) \quad (8)$$

rolling constraint

Due to the free rotation of rollers, an additional term of $\dot{\varphi}_{sw}$ is added.

$$\dot{x}_w = r\dot{\varphi}\sin(\gamma) + r_{sw}\dot{\varphi}_{sw} \quad (9)$$

sliding constraint

$$\mathrm{w}^v IW = \mathrm{w}^v IR + \mathrm{w}^\omega IR * \mathrm{w}^r RS \quad (10)$$

$$\mathrm{w}^v IW = \begin{bmatrix} r\,\dot{\varphi}\sin(\gamma) + r_{SW}\,\dot{\varphi}_{SW} \\ r\,\dot{\varphi}\cos(\gamma) \\ 0 \end{bmatrix} \quad (11)$$

$$\mathrm{w}^v IR = R_{sw}\,R_{SR}\,R_{RI}\begin{bmatrix} \dot{x} \\ \dot{y} \\ 0 \end{bmatrix} = \mathrm{R}(\alpha+\beta+\gamma)\ \mathrm{R}(\Theta)\begin{bmatrix} \dot{x} \\ \dot{y} \\ 0 \end{bmatrix} \quad (12)$$

$$\mathrm{R}(\alpha+\beta+\gamma) = \begin{bmatrix} \cos(\alpha+\beta+\gamma) & \sin(\alpha+\beta+\gamma) & 0 \\ -\sin(\alpha+\beta+\gamma) & \cos(\alpha+\beta+\gamma) & 0 \\ 0 & 0 & 1 \end{bmatrix} \quad (13)$$

$$\mathrm{w}^\omega IR * \mathrm{w}^r RS = \begin{bmatrix} 0 & -\dot{\theta} & 0 \\ \dot{\theta} & 0 & 0 \\ 0 & 0 & 0 \end{bmatrix}\begin{bmatrix} l\cos(\beta+\gamma) \\ -l\sin(\beta+\gamma) \\ 0 \end{bmatrix} = \begin{bmatrix} l\sin(\beta) \\ l\cos(\beta) \\ 0 \end{bmatrix}\dot{\theta} \quad (14)$$

The rolling constraint of the wheel is:

$$[-\sin(\alpha+\beta+\gamma)\cos(\alpha+\beta+\gamma)\ \ l\cos(\beta+\gamma)]\,R(\theta)\,\dot{\xi}_1 - r\dot{\varphi}\cos(\gamma) = 0 \quad (15)$$

$$[\cos(\alpha+\beta+\gamma)\ \ \sin(\alpha+\beta+\gamma)\ \ l\sin(\beta+\gamma)](\theta)\,\dot{\xi}_1 - r\dot{\varphi}\sin(\gamma) + r_{sw}\dot{\varphi}_{sw} = 0 \quad (16)$$

Mecanum wheel specifications

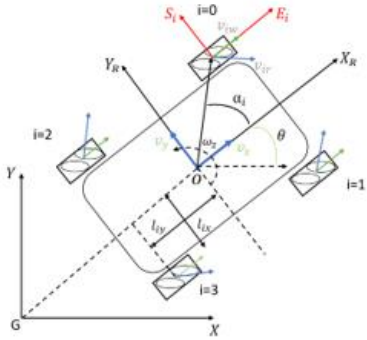

Considering $l_{ix} = l_i \cos a_i$ and $l_{iy} = l_i \sin a_i$ (17)

Assuming the wheels are the same size, the transformation matrix is

$$T = \frac{1}{-r}\begin{bmatrix} \frac{\cos(\beta_i + \mathrm{y}_i)}{\sin(\mathrm{y}_i)} & \frac{\sin(\beta_i + \mathrm{y}_i)}{\sin(\mathrm{y}_i)} & \frac{l_i\sin(-\alpha_i+\beta_i-\mathrm{y}_i)}{\sin(\mathrm{y}_i)} \\ -\frac{r\cos(\beta_i)}{\sin(\mathrm{y}_i)} & -\frac{r\sin(\beta_i)}{\sin(\mathrm{y}_i)} & -\frac{l_i\sin(-\alpha_i+\beta_i)r}{\sin(\mathrm{y}_i)} \end{bmatrix}; \quad (18)$$

$$\mathrm{r}^+ = \frac{1}{l_i^2+1}\begin{bmatrix} -\frac{1}{2}(l_i^2\sin(\beta_i) - l_i^2\sin(-\beta_i+2\alpha_i) + 2\sin(\beta_i))r & \frac{1}{2}l_i^2\sin(\mathrm{y}_i-\beta_i+2\alpha_i) - \frac{1}{2}\sin(-\mathrm{y}_i+\beta_i)l_i^2 - \sin(-\mathrm{y}_i+\beta_i) \\ \frac{1}{2}r(l_i^2\cos(\beta_i) - l_i^2\cos(-\beta_i+2\alpha_i) + 2\cos(\beta_i)) & -\frac{1}{2}l_i^2\cos(\mathrm{y}_i-\beta_i+2\alpha_i) + \frac{1}{2}\cos(-\mathrm{y}_i+\beta_i)l_i^2 + \cos(-\mathrm{y}_i+\beta_i) \\ \cos(\alpha_i-\beta_i)l_i\mathrm{r} & \cos(\alpha_i-\beta_i+\mathrm{y}_i)l_i \end{bmatrix} \quad (19)$$

Since the relation between independent variables virand in each joint and the system angular and linear velocity, assuming no wheel slipping on the ground, the inverse kinematic model can be

$$\begin{bmatrix}\omega_1\\ \omega_2\\ \omega_3\\ \omega_4\end{bmatrix}=\frac{1}{-r}\begin{bmatrix}\frac{\cos(\beta_1-\gamma_1)}{\sin\gamma_1} & \frac{\sin(\beta_1-\gamma_1)}{\sin\gamma_1} & \frac{l_1\sin(\beta_1-\gamma_1-\alpha_1)}{\sin\gamma_1}\\ \frac{\cos(\beta_2-\gamma_2)}{\sin\gamma_2} & \frac{\sin(\beta_2-\gamma_2)}{\sin\gamma_2} & \frac{l_2\sin(\beta_2-\gamma_2-\alpha_2)}{\sin\gamma_2}\\ \frac{\cos(\beta_3-\gamma_3)}{\sin\gamma_3} & \frac{\sin(\beta_3-\gamma_3)}{\sin\gamma_3} & \frac{l_3\sin(\beta_3-\gamma_3-\alpha_3)}{\sin\gamma_3}\\ \frac{\cos(\beta_4-\gamma_4)}{\sin\gamma_4} & \frac{\sin(\beta_4-\gamma_4)}{\sin\gamma_4} & \frac{l_4\sin(\beta_4-\gamma_4-\alpha_4)}{\sin\gamma_4}\end{bmatrix}\begin{bmatrix}v_X\\ v_Y\\ \omega_Z\end{bmatrix} \quad (20)$$

Inverse kinematics in the Jacobian form

$$T=\frac{1}{-r}\begin{bmatrix}\frac{\cos(\beta_1-\gamma_1)}{\sin\gamma_1} & \frac{\sin(\beta_1-\gamma_1)}{\sin\gamma_1} & \frac{l_1\sin(\beta_1-\gamma_1-\alpha_1)}{\sin\gamma_1}\\ \frac{\cos(\beta_2-\gamma_2)}{\sin\gamma_2} & \frac{\sin(\beta_2-\gamma_2)}{\sin\gamma_2} & \frac{l_2\sin(\beta_2-\gamma_2-\alpha_2)}{\sin\gamma_2}\\ \frac{\cos(\beta_3-\gamma_3)}{\sin\gamma_3} & \frac{\sin(\beta_3-\gamma_3)}{\sin\gamma_3} & \frac{l_3\sin(\beta_3-\gamma_3-\alpha_3)}{\sin\gamma_3}\\ \frac{\cos(\beta_4-\gamma_4)}{\sin\gamma_4} & \frac{\sin(\beta_4-\gamma_4)}{\sin\gamma_4} & \frac{l_4\sin(\beta_4-\gamma_4-\alpha_4)}{\sin\gamma_4}\end{bmatrix} \quad (21)$$

And the forward kinematics.

$$\begin{bmatrix}v_X\\ v_Y\\ \omega_Z\end{bmatrix} = \mathrm{T}^{+}\begin{bmatrix}\omega_1\\ \omega_2\\ \omega_3\\ \omega_4\end{bmatrix} \quad (22)$$

For four mecanum omnidirectional solutions, the parameters of this configuration are in the following Table

i	wheels	α_i	β_i	γ_i	l_i	l_{ix}	l_{iy}
0	1SW	$\frac{\pi}{4}$	$\frac{\pi}{2}$	$\frac{-\pi}{4}$	l	l_x	l_y
1	2SW	$\frac{-\pi}{4}$	$\frac{-\pi}{2}$	$\frac{\pi}{4}$	l	l_x	l_y
2	3SW	$\frac{3\pi}{4}$	$\frac{\pi}{2}$	$\frac{\pi}{4}$	l	l_x	l_y
0	4SW	$\frac{-3\pi}{4}$	$\frac{-\pi}{2}$	$\frac{-\pi}{4}$	l	l_x	l_y

By replacing the parameters from the Table with the matrix

$$T=\frac{1}{r}\begin{bmatrix}1 & -1 & -(l_x+l_y)\\ 1 & 1 & (l_x+l_y)\\ 1 & 1 & -(l_x+l_y)\\ 1 & -1 & (l_x+l_y)\end{bmatrix} \quad (23)$$

$$\mathrm{T}^{+}=\frac{r}{4}\begin{bmatrix}1 & 1 & 1 & 1\\ -1 & 1 & 1 & -1\\ -\frac{1}{(l_x+l_y)} & \frac{1}{(l_x+l_y)} & -\frac{1}{(l_x+l_y)} & \frac{1}{(l_x+l_y)}\end{bmatrix}; \quad (24)$$

Therefore, the inverse kinematics

$$\begin{bmatrix}\omega_1\\ \omega_2\\ \omega_3\\ \omega_4\end{bmatrix}=\frac{1}{r}\begin{bmatrix}1 & -1 & -(l_x+l_y)\\ 1 & 1 & (l_x+l_y)\\ 1 & 1 & -(l_x+l_y)\\ 1 & -1 & (l_x+l_y)\end{bmatrix}\begin{bmatrix}v_X\\ v_Y\\ \omega_Z\end{bmatrix} \quad (25)$$

$$\omega_1=\frac{1}{r}(v_X - v_Y - (l_x+l_y)\omega), \quad (26)$$

$$\omega_2=\frac{1}{r}(v_X + v_Y + (l_x+l_y)\omega), \quad (27)$$

$$\omega_3=\frac{1}{r}(v_X + v_Y - (l_x+l_y)\omega), \quad (28)$$

$$\omega_4=\frac{1}{r}(v_X - v_Y + (l_x+l_y)\omega). \quad (29)$$

And the forward kinematics

$$\begin{bmatrix}v_X\\ v_Y\\ \omega_Z\end{bmatrix}=\frac{r}{4}\begin{bmatrix}1 & 1 & 1 & 1\\ -1 & 1 & 1 & -1\\ -\frac{1}{(l_x+l_y)} & \frac{1}{(l_x+l_y)} & -\frac{1}{(l_x+l_y)} & \frac{1}{(l_x+l_y)}\end{bmatrix}\begin{bmatrix}\omega_1\\ \omega_2\\ \omega_3\\ \omega_4\end{bmatrix} \quad (30)$$

R	0.05m
Lx	0.026m
Ly	0.026m

RESULTS

Experiment is conducted using our mobile manipulator experimental setup shown in Figure 5. To verify the effectiveness of proposed controllers and highlight the benefits of the mechanical wheel mechanism.

A pen is installed in the center of gravity (CG) of the robot's chassis to following a circular path with a circle diameter of 2-meter Figure 5.

Figure 5. path following experiment

The result of the circular path following the robot in figure 5.

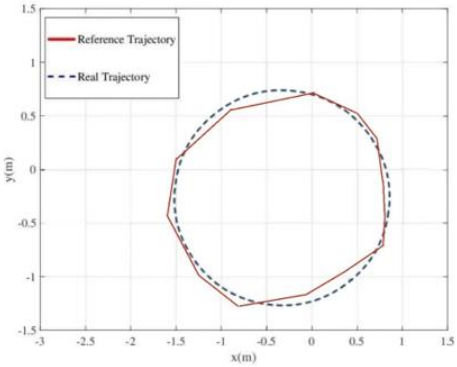

Figure 5. circular path following.

The second experiment uses the motor's encoder to extract the PWM VS Y_ distance and PWM VS X Distance Both for large motor and small motor as follows:

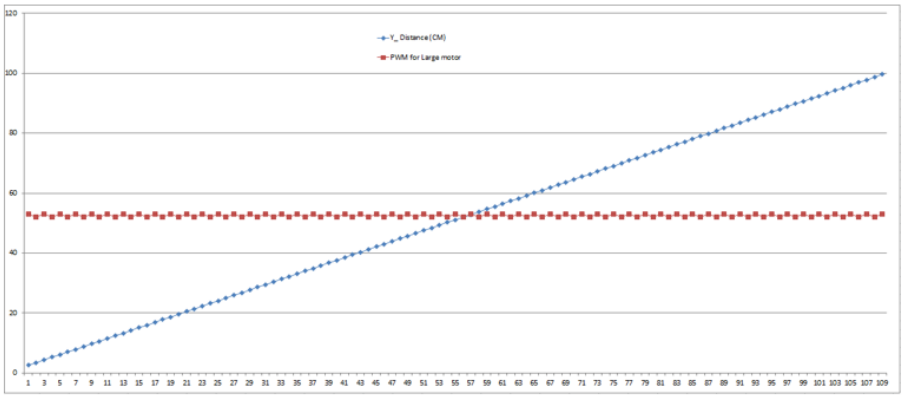

Figure 6. PWM large motor VS Y distance.

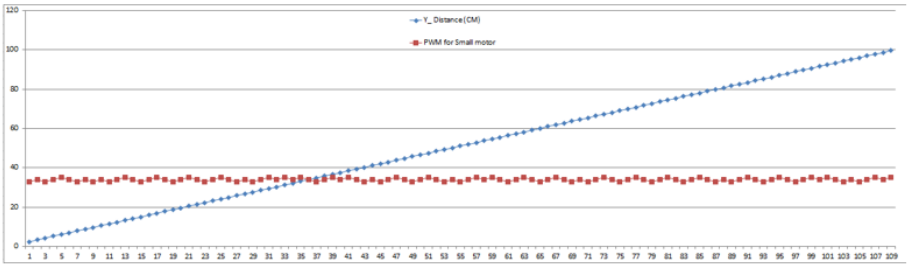

Figure 7. PWM small motor VS Y distance.

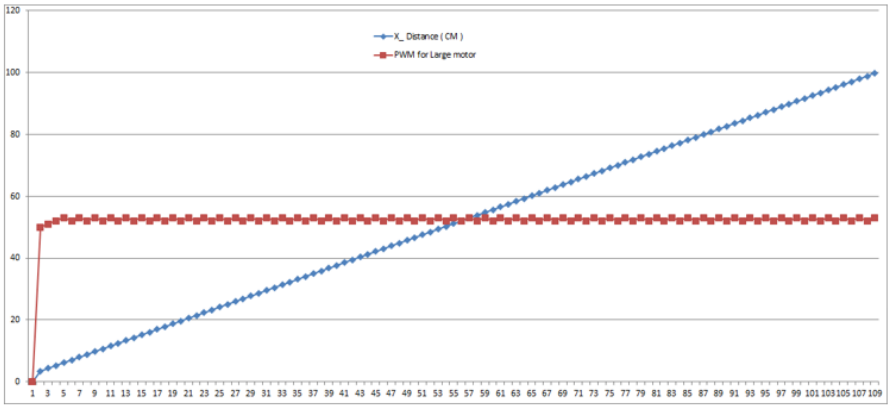

Figure 8. PWM large motor VS X distance.

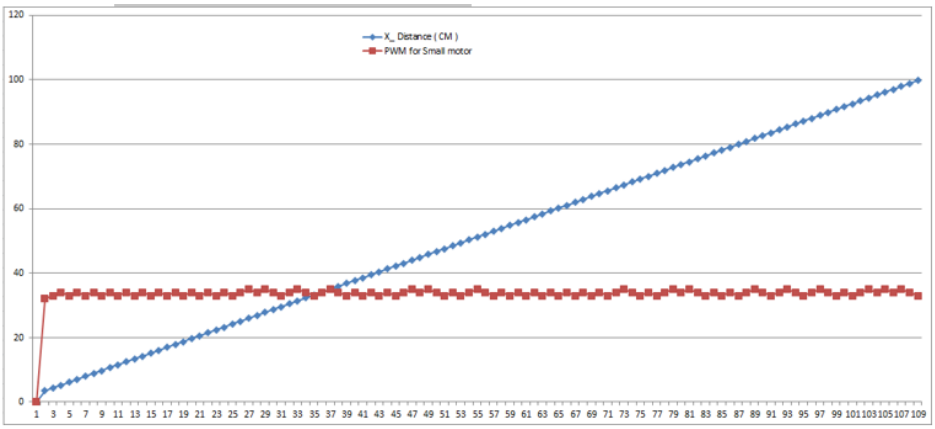

Figure 9. PWM small motor VS X distance

4. CONCLUSIONS

This study examines the compatibility of a holonomic wheeled mobile robot with four Mecanum wheels with its intended and theoretical pathways. For the purpose of researching the kinematics and route tracking for this kind of WMR, a real-world prototype model has been created. The WMR makes slight mistakes while following a circular course in the first trial, and the second experiment demonstrates the scope of the control system's strength and precision as well as the relationship between big and tiny motors. The outcomes of two studies demonstrated good agreement between desired and actual route tracking and confirmed that the errors in the x, y, and orientation are within acceptable bounds

5. REFERENCES

[1] Fang, Y., Qi, J., Hu, J., Wang, W., & Peng, Y. (2020). An approach for jerk-continuous trajectory generation of robotic manipulators with kinematical constraints. Mechanism and Machine Theory, 153, 103957. https://doi.org/10.1016/j.mechmachtheory.2020.103957 .

[2] Ananthanarayanan, H., & Ordóñez, R. (2015). Real-time Inverse Kinematics of (2n + 1) DOF hyper-redundant manipulator arm via a combined numerical and analytical approach. Mechanism and Machine Theory, 91, 209–226. https://doi.org/10.1016/j.mechmachtheory.2015.04.011.

[3] Duka, A.-V. (2014). Neural Network based Inverse Kinematics Solution for Trajectory Tracking of a Robotic Arm. *Procedia Technology*, *12*, 20–27. https://doi.org/10.1016/j.protcy.2013.12.451

[4] Lee, S., & Bejczy, A. K. (1991). *Redundant Arm Kinematic Control Based on Parameterization*.

[5] Zaplana, I., & Basanez, L. (n.d.). *A novel closed-form solution for the inverse kinematics of redundant manipulators through workspace analysis*.

[6] Joublin, F. (1997). Closed form solution for the inverse kinematics of a redundant robot arm. https://www.researchgate.net/publication/239460298

[7] Shimizu, M., Kakuya, H., Yoon, W. K., Kitagaki, K., & Kosuge, K. (2008). Analytical inverse kinematic computation for 7-DOF redundant manipulators with joint limits and its application to redundancy resolution. *IEEE Transactions on Robotics*, *24*(5), 1131–1142. https://doi.org/10.1109/TRO.2008.2003266

[8] Yan, L., Mu, Z., Xu, W., & Member, I. (n.d.). *Analytical Inverse Kinematics of a Class of Redundant Manipulator Based on Dual Arm-Angle Parameterization*.

[9] Tian, X., Xu, Q., & Zhan, Q. (2020). An analytical inverse kinematics solution with joint limits avoidance of 7-DOF anthropomorphic manipulators without offset. Journal of the Franklin Institute, xxxx, 1–21. https://doi.org/10.1016/j.jfranklin.2020.11.020

[10] Illah, R. (n.d.). *Autonomous Mobile Robots Introduction to SIEGWART NOURBAKHSH Contents Acknowledgments xi*.

[11] Lopez-Franco, C., Hernandez-Barragan, J., Alanis, A. Y., & Arana-Daniel, N. (2018). A soft computing approach for inverse kinematics of robot manipulators. *Engineering Applications of Artificial Intelligence*, *74*(June), 104–120. https://doi.org/10.1016/j.engappai.2018.06.001

[12] Dhyani, A., Panda, M. K., & Jha, B. (2020). Design of an evolving Fuzzy-PID controller for optimal trajectory control of a 7-DOF redundant manipulator with prioritized sub-tasks. *Expert Systems with Applications*, *162*(xxxx), 113021. https://doi.org/10.1016/j.eswa.2019.113021

[13] Baghli, F. Z., Bakkali, L. El, & Lakhal, Y. (2017). Optimization of Arm Manipulator Trajectory Planning in the Presence of Obstacles by Ant Colony Algorithm. Procedia Engineering, 181, 560–567. https://doi.org/10.1016/j.proeng.2017.02.434

[14] Staal, A. S., Salvatierra, C. G., Albertsen, D. D., Mahendran, M., Ravichandran, R., Thomsen, R. F., Hansen, E. B., & Bogh, S. (2020). Towards a collaborative omnidirectional mobile robot in a smart cyber-physical environment. Procedia Manufacturing, 51, 193 200.doi.org/10.1016/j.promfg.2020.10.028

[15] Mellah, S., Graton, G., Mostafa, E., Adel, E. L., Ouladsine, M., & Planchais, A. (2020). 4-mecanum wheeled mobile robot actuator fault detection & isolation using unknown input observer-based approach. https://doi.org/10.0/Linux-x86_64

[16] Mishra, S., Sharma, M., & Santhakumar, M. (2019). Behavioural fault-tolerant-control of an omni-directional mobile robot with four-mecanum wheels.

Defence Science Journal, 69(4), 353–360. https://doi.org/10.14429/dsj.69.13607

[17] Savaee, E., & Hanzaki, A. R. (n.d.). A New Algorithm for Calibration of an Omni-Directional Wheeled Mobile Robot Based on Effective Kinematic Parameters Estimation. https://doi.org/10.1007/s10846-020-01296-9/Published

[18] Institute of Electrical and Electronics Engineers. (n.d.). *2019 IEEE International Conference on Systems, Man and Cybernetics (SMC) : Bari, Italy. October 6-9, 2019.*

[19] Hasan, S. F., & Alwan, H. M. (2021). Enhancing Tilt-Integral-Derivative Controller to Motion Control of Holonomic Wheeled Mobile Robot by Using New Hybrid Approach. *IOP Conference Series: Materials Science and Engineering*, *1094*(1), 012097. https://doi.org/10.1088/1757-899x/1094/1/012097

[20] Wang, D., Wei, W., Yeboah, Y., Li, Y., & Gao, Y. (2020). A Robust Model Predictive Control Strategy for Trajectory Tracking of Omni-directional Mobile Robots. *Journal of Intelligent and Robotic Systems: Theory and Applications*, *98*(2), 439–453. https://doi.org/10.1007/s10846-019-01083-1

[21] Mellah, S., Graton, G., el Adel, E. M., Ouladsine, M., & Planchais, A. (2021). Health State Monitoring of 4-mecanum Wheeled Mobile Robot Actuators and its Impact on the Robot Behavior Analysis. *Journal of Intelligent and Robotic Systems: Theory and Applications*, *102*(4). https://doi.org/10.1007/s10846-021-01446-7

[22] Khnissi, K., Ben Jabeur, C., & Seddik, H. (2020). A smart mobile robot commands predictor using recursive neural network. *Robotics and Autonomous Systems*, *131*, 103593. https://doi.org/10.1016/j.robot.2020.103593

[23] Suárez, R., Palomo-Avellaneda, L., Martinez, J., Clos, D., & García, N. (2018). Development of a Dexterous Dual-Arm Omnidirectional Mobile Manipulator. *IFAC-PapersOnLine*, *51*(22), 126–131. https://doi.org/10.1016/j.ifacol.2018.11.529

[24] Lakshmi Srinivas, G., & Javed, A. (2020).Topology optimization of rigid-links for industrial manipulator considering dynamic loading conditions.*Mechanism and Machine Theory*, *153*, 103979. https://doi.org/10.1016/j.mechmachtheory.2020.103979

[25] Alebooyeh, M., & Urbanic, R. J. (2019). Neural Network Model for Identifying Workspace, Forward and Inverse Kinematics of the 7-DOF YuMi 14000 ABB Collaborative Robot. *IFAC-PapersOnLine*, *52*(10), 176–181. https://doi.org/10.1016/j.ifacol.2019.10.019

[26] Bae, J., Bak, J., Jin, S., Seo, T. W., & Kim, J. (2018). Optimal configuration and parametric design of an underwater vehicle manipulator system for a valve task. *Mechanism and Machine Theory*, *123*, 76–88. https://doi.org/10.1016/j.mechmachtheory.2018.01.014

[27] Jiokou Kouabon, A. G., Melingui, A., Mvogo Ahanda, J. J. B., Lakhal, O., Coelen, V., KOM, M., & Merzouki, R. (2020). A Learning Framework to inverse kinematics of high DOF redundant manipulators. *Mechanism and Machine Theory*, *153*, 103978. https://doi.org/10.1016/j.mechmachtheory.2020.103978